INTERNATIONAL JOURNAL FOR NUMERICAL METHODS IN FLUIDS
*Int. J. Numer. Meth. Fluids* 2006; **50**:275–307
Published online 1 September 2005 in Wiley InterScience (www.interscience.wiley.com). DOI: 10.1002/fld.1055

# A Riemann solver and upwind methods for a two-phase flow model in non-conservative form

C. E. Castro*,† and E. F. Toro‡

*Laboratory of Applied Mathematics, Faculty of Engineering, University of Trento, Trento, Italy*

SUMMARY

We present a theoretical solution for the Riemann problem for the five-equation two-phase non-conservative model of Saurel and Abgrall. This solution is then utilized in the construction of upwind non-conservative methods to solve the general initial-boundary value problem for the two-phase flow model in non-conservative form. The basic upwind scheme constructed is the non-conservative analogue of the Godunov first-order upwind method. Second-order methods in space and time are then constructed via the MUSCL and ADER approaches. The methods are systematically assessed via a series of test problems with theoretical solutions. Copyright © 2005 John Wiley & Sons, Ltd.

KEY WORDS: two-phase flow; non-conservative form; hyperbolic equations; Riemann solver; non-conservative upwind methods

## 1. INTRODUCTION

Mathematical modelling of multi-phase-flow phenomena is currently a very active field of research. The mathematical models have application in many fields, such as Deflagration to Detonation Transition (DDT) in combustion theory, Self-propagating High-temperature Synthesis (SHS), nuclear engineering, environmental disciplines, the oil industry, and many more. The underlying physics of the problems is complex and the aim of the mathematical models is to account for the behaviour of at least two phases or fluids and the interactions due to exchange of mass, momentum and energy. A large class of models are based on the continuum

*Correspondence to: C. E. Castro, Laboratory of Applied Mathematics, Faculty of Engineering, University of Trento, Via Mesiano 77, Trento 38050, Italy.
†E-mail: castroc@ing.unitn.it
‡E-mail: toro@ing.unitn.it

Contract/grant sponsor: University of Trento
Contract/grant sponsor: University of Cambridge
Contract/grant sponsor: EPSRC; contract/grant number: GRN09276

*Received 23 December 2004*
*Revised 10 May 2005*
*Accepted 18 May 2005*

theory and make use of average quantities [1–4] inside each control volume allowing us to know the amount of each phase in the volume but not the position of the interphases. Models in current use, when neglecting dissipative effects, consist of non-linear systems of first-order partial differential equations along with closure conditions. There are at present two important issues regarding these models. The first of these refers to the hyperbolic or non-hyperbolic character of the equations. It is now established that hyperbolicity is an essential requirement to have well-posedness [1]. The second issue concerns the conservative or non-conservative character of the equations, that is to say, whether the governing equations have, or not, a known conservation-law form in the mathematical sense. In the absence of a conservative form of the equations one speaks of non-conservative model, even though in the derivation of the equations one invokes physical conservation principles. Mathematically, shock waves and associated Rankine–Hugoniot conditions can be defined once a conservative form of the equations exists.

Almost all the models in the literature have non-conservative form due to the interface interaction. Examples include the Saurel–Abgrall model [5] and the Baer–Nunziato model [6]. See also Reference [1]. We note here that conservative hyperbolic models have recently been proposed [7], which are formulated in terms of parameters of state for the mixture. Given that most models in current use are in non-conservative form, it is of interest to develop numerical methodology that can be applied to solve such systems of hyperbolic equations in non-conservative form.

In this paper we consider the hyperbolic non-conservative model of Saurel and Abgrall [5]. We solve the Riemann problem for this five-equation model approximately assuming that all non-linear characteristic fields give rise to rarefaction waves. We call the approximation, the *four-rarefaction approximation*, and is an extension of the two-rarefaction approximation in single-phase gas dynamics [8]. The solution has close form and is actually exact in the case in which the Riemann problem has four rarefaction waves. For other cases our theoretical solution becomes an approximation. Careful assessment of the approximate theoretical solution indicates that this is sufficiently accurate for use in the construction of upwind numerical methods. We note here that our theoretical solution is direct, unlike that presented by Andrianov [9] for the more complicated Baer–Nunziato model. Our Riemann solver is *complete*, in that it accounts for all waves present in the eigenstructure of the exact solution. Our solver is also nonlinear and therefore avoids typical problems of standard linearized Riemann solvers concerning low-densities flows, sonic flows and strong shock waves.

The second contribution of this paper is the construction of non-conservative upwind numerical methods that use locally the four-rarefaction Riemann solver. We construct a non-conservative analogue of the Godunov first-order upwind method. We also construct second-order nonlinear schemes using the TVD approach and the ENO approach.

The rest of this article is organized as follows: in Section 2 we review the mathematical model of Saurel and Abgrall and present two possible formulations for it. In Section 3 we study the eigenstructure of the system for both formulations and find the generalized Riemann invariants. In Section 4 an approximate Riemann solver is developed. In Section 5 we construct three upwind numerical methods and in Section 6 we present numerical results and discuss the performance of the numerical methods, the solutions of which are compared with the theoretical solution of this paper. Conclusions are drawn in Section 7.

 

## 2. GOVERNING EQUATIONS

In this section we study the isentropic two phase flow model of Saurel and Abgrall [5] that governs the dynamics of two compressible fluids (called *phases*, hereafter), such as gas and liquid.

### 2.1. The closed model

The Saurel–Abgrall model [5] for the mixture of two compressible fluids neglecting mass transfer and drag force, in terms of conserved variables, reads as

$$\frac{\partial}{\partial t}(\alpha_{\mathrm{g}}\rho_{\mathrm{g}}) + \frac{\partial}{\partial x}(\alpha_{\mathrm{g}}\rho_{\mathrm{g}}u_{\mathrm{g}}) = S_1 \tag{1}$$

$$\frac{\partial}{\partial t}(\alpha_{\mathrm{g}}\rho_{\mathrm{g}}u_{\mathrm{g}}) + \frac{\partial}{\partial x}(\alpha_{\mathrm{g}}\rho_{\mathrm{g}}u_{\mathrm{g}}^2 + \alpha_{\mathrm{g}}p_{\mathrm{g}}) - p_i\frac{\partial}{\partial x}\alpha_{\mathrm{g}} = S_2 \tag{2}$$

$$\frac{\partial}{\partial t}(\alpha_{\mathrm{l}}\rho_{\mathrm{l}}) + \frac{\partial}{\partial x}(\alpha_{\mathrm{l}}\rho_{\mathrm{l}}u_{\mathrm{l}}) = S_3 \tag{3}$$

$$\frac{\partial}{\partial t}(\alpha_{\mathrm{l}}\rho_{\mathrm{l}}u_{\mathrm{l}}) + \frac{\partial}{\partial x}(\alpha_{\mathrm{l}}\rho_{\mathrm{l}}u_{\mathrm{l}}^2 + \alpha_{\mathrm{l}}p_{\mathrm{l}}) + p_i\frac{\partial}{\partial x}\alpha_{\mathrm{g}} = S_4 \tag{4}$$

$$\frac{\partial}{\partial t}\alpha_{\mathrm{g}} + \lambda\frac{\partial}{\partial x}\alpha_{\mathrm{g}} = 0 \tag{5}$$

Here $\alpha_k$ is the volume fraction of phase $k$, $k=\mathrm{g}$ (gas) and $k=\mathrm{l}$ (liquid); $\rho_k$ is the density of phase $k$; $u_k$ is the velocity of phase $k$, $p_k$ is the pressure of phase $k$, $\lambda$ is an *interphase* speed and $p_i$ an *interphase* pressure. Equations (1)–(4) express the laws of conservation of mass and momentum for each phase. Equation (5) is an advection equation for the gas volume fraction, where the advection speed is $\lambda$. As in the article by Saurel–Abgrall [5], the interphase speed and the interface pressure are defined as

$$\lambda = \frac{\sum \alpha_k\rho_k u_k}{\sum \alpha_k\rho_k}, \quad p_i = \sum \alpha_k p_k, \ \ k=\mathrm{g},\mathrm{l} \tag{6}$$

Other possibilities have also been proposed in the last few years, see for example References [10, 11].

A distinctive feature of system (1)–(5) is that although it is based on the physical conservation principles of mass and momentum and it is expressed in terms of the conserved variables, the mathematical form of (1)–(5) is *not conservative*, or equivalently, the system is not in divergence form. Moreover, to our knowledge system (1)–(5) cannot be cast in conservative or divergence form.

To close system (1)–(5) we need to define the pressures $p_{\mathrm{g}}$, $p_{\mathrm{l}}$ via appropriate equations of state. Here we choose isentropic laws of the form

$$p_{\mathrm{g}} = p_{\mathrm{g}}(\rho_{\mathrm{g}}), \quad p_{\mathrm{l}} = p_{\mathrm{l}}(\rho_{\mathrm{l}}) \tag{7}$$

In particular for the gas phase we take

$$p_{\mathrm{g}} = p_{\mathrm{g}}(\rho_{\mathrm{g}}) = K_{\mathrm{g}}\rho_{\mathrm{g}}^{\gamma_{\mathrm{g}}} \tag{8}$$

 

where $K_g$ and $\gamma_g$ are constants to be specified. For the liquid phase we use the Tait's [12] equation of state

$$p_l = p_l(\rho_l) = K_l \left[ \left( \frac{\rho_l}{\rho_o} \right)^{\gamma_l} - 1 \right] \tag{9}$$

where $K_l$, $\gamma_l$ and $\rho_o$ are constants, also to be specified.

### 2.2. Formulations

Here we derive two formulations of the governing equations, based on two choices of variables. Equations (1)–(5) with $S_i = 0$ $(i = 1, \ldots, 4)$ can be cast in quasi-linear form as

$$\partial_t Q + A(Q)\partial_x Q = 0 \tag{10}$$

where

$$Q = [\alpha_g \rho_g,\ \alpha_g \rho_g u_g,\ \alpha_l \rho_l,\ \alpha_l \rho_l u_l,\ \alpha_g]^T \tag{11}$$

is the vector of conserved variables and the coefficient matrix $A(Q)$ is

$$A(Q) = \begin{bmatrix} 0 & 1 & 0 & 0 & 0 \\ a_g^2 - u_g^2 & 2u_g & 0 & 0 & p_g(1-\gamma_g) - p_i \\ 0 & 0 & 0 & 1 & 0 \\ 0 & 0 & a_l^2 - u_l^2 & 2u_l & p_l(\gamma_l - 1) + p_i + K_l\gamma_l \\ 0 & 0 & 0 & 0 & \lambda \end{bmatrix} \tag{12}$$

which can be easily verified by expanding the spatial derivatives of products and algebraic manipulations. The matrix contains the sound speeds of both phases

$$\begin{aligned} a_g &= \sqrt{\frac{\gamma_g p_g}{\rho_g}} \\ a_l &= \sqrt{\frac{\gamma_l}{\rho_l}(p_l + K_l)} \end{aligned} \tag{13}$$

An alternative choice of variables, and formulations, is the vector of primitive or physical variables

$$W = [\rho_g,\ u_g,\ \rho_l,\ u_l,\ \alpha_g]^T \tag{14}$$

for which the governing equations take the form

$$\partial_t W + A(W)\partial_x W = 0 \tag{15}$$

 

where the coefficient matrix is

$$A(W)=\begin{bmatrix} u_g & \rho_g & 0 & 0 & \dfrac{\rho_g(u_g-\lambda)}{\alpha_g} \\ \dfrac{a_g^2}{\rho_g} & u_g & 0 & 0 & \dfrac{p_g-p_i}{\alpha_g\rho_g} \\ 0 & 0 & u_l & \rho_l & \dfrac{\rho_l(\lambda-u_l)}{\alpha_l} \\ 0 & 0 & \dfrac{a_l^2}{\rho_l} & u_l & \dfrac{p_i-p_l}{\alpha_l\rho_l} \\ 0 & 0 & 0 & 0 & \lambda \end{bmatrix} \tag{16}$$

## 3. EIGENSTRUCTURE AND GENERALIZED RIEMANN INVARIANTS

In this section we establish the eigenstructure of the systems (10), (15) and derive the generalized Riemann invariants [13]; these will be utilized in Section 4 for finding an approximate solution to the Riemann problem. For both formulations (10), (15) the eigenvalues are

$$\lambda_1=u_l-a_l,\quad \lambda_2=u_g-a_g,\quad \lambda_3=\lambda,\quad \lambda_4=u_g+a_g,\quad \lambda_5=u_l+a_l \tag{17}$$

The corresponding right eigenvectors differ for each formulation. For the primitive-variable formulation (15) the right eigenvectors are:

$$R^{(1)}=\begin{bmatrix} 0 \\ 0 \\ -\rho_l \\ a_l \\ 0 \end{bmatrix},\quad R^{(2)}=\begin{bmatrix} -\rho_g \\ a_g \\ 0 \\ 0 \\ 0 \end{bmatrix},\quad R^{(4)}=\begin{bmatrix} \rho_g \\ a_g \\ 0 \\ 0 \\ 0 \end{bmatrix},\quad R^{(5)}=\begin{bmatrix} 0 \\ 0 \\ \rho_l \\ a_l \\ 0 \end{bmatrix} \tag{18}$$

$$R^{(3)}=\begin{bmatrix} -\dfrac{1}{\alpha_g}\dfrac{p_i-p_g+\rho_g(u_g-\lambda)^2}{(u_g-\lambda)^2-a_g^2} \\ -\dfrac{1}{\alpha_g\rho_g}\dfrac{(\lambda-u_g)(\rho_g a_g^2-p_g+p_i)}{(u_g-\lambda)^2-a_g^2} \\ \dfrac{1}{\alpha_l}\dfrac{p_i-p_l+\rho_l(u_l-\lambda)^2}{(u_l-\lambda)^2-a_l^2} \\ \dfrac{1}{\alpha_l\rho_l}\dfrac{(\lambda-u_l)(\rho_l a_l^2-p_l+p_i)}{(u_l-\lambda)^2-a_l^2} \\ 1 \end{bmatrix} \tag{19}$$

 

For the conserved-variable formulation (10) the right eigenvectors are:

$$R^{(1)}=\begin{bmatrix}0\\0\\1\\u_{\mathrm{l}}-a_{\mathrm{l}}\\0\end{bmatrix},\quad R^{(2)}=\begin{bmatrix}1\\u_{\mathrm{g}}-a_{\mathrm{g}}\\0\\0\\0\end{bmatrix},\quad R^{(4)}=\begin{bmatrix}1\\u_{\mathrm{g}}+a_{\mathrm{g}}\\0\\0\\0\end{bmatrix},\quad R^{(5)}=\begin{bmatrix}0\\0\\1\\u_{\mathrm{l}}+a_{\mathrm{l}}\\0\end{bmatrix} \tag{20}$$

$$R^{(3)}=\begin{bmatrix}\dfrac{p_{\mathrm{g}}(\gamma-1)+p_i}{a_{\mathrm{g}}^2-(u_{\mathrm{g}}-\lambda)^2}\\[2ex]\lambda\,\dfrac{p_{\mathrm{g}}(\gamma_{\mathrm{g}}-1)+p_i}{a_{\mathrm{g}}^2-(u_{\mathrm{g}}-\lambda)^2}\\[2ex]\dfrac{p_{\mathrm{l}}(1-\gamma_{\mathrm{l}})-p_i-K_{\mathrm{l}}\gamma_{\mathrm{l}}}{a_{\mathrm{l}}^2-(u_{\mathrm{l}}-\lambda)^2}\\[2ex]\lambda\,\dfrac{p_{\mathrm{l}}(1-\gamma_{\mathrm{l}})-p_i-K_{\mathrm{l}}\gamma_{\mathrm{l}}}{a_{\mathrm{l}}^2-(u_{\mathrm{l}}-\lambda)^2}\\[2ex]1\end{bmatrix} \tag{21}$$

With the eigenvalues and eigenvectors available we establish the nature of the characteristic fields associated with each pair $(\lambda_i,\ R^{(i)})$. For example, the characteristic field associated with $\lambda_3=\lambda$ is seen to be linearly degenerate as

$$\nabla\lambda_3(W)\cdot R^{(3)}(W)=0\quad\forall W \tag{22}$$

The remaining characteristic fields are all genuinely non-linear as

$$\nabla\lambda_k(W)\cdot R^{(k)}(W)\neq 0\quad\forall W \tag{23}$$

The generalized Riemann invariants are used to establish useful relations across simple waves connecting two constant states. Consider an $n\times n$ system with unknowns $W=[w_1\ldots w_n]^{\mathrm{T}}$, for which given an eigenvalue $\lambda_k$ and its corresponding eigenvector

$$R^{(k)}(W)=[r_1^{(k)},\ldots,r_n^{(k)}]^{\mathrm{T}}$$

the corresponding generalized Riemann invariants are [13]

$$\frac{\mathrm{d}w_1}{r_1^{(k)}}=\frac{\mathrm{d}w_2}{r_2^{(k)}}=\cdots=\frac{\mathrm{d}w_n}{r_n^{(k)}}$$

From here one obtains $(n-1)$ ordinary differential equations in phase space. Now assume two constant states $W_L=[\rho_{\mathrm{g}L},\ u_{\mathrm{g}L},\ \rho_{\mathrm{l}L},\ u_{\mathrm{l}L},\ \alpha_{\mathrm{g}L}]^{\mathrm{T}}$ and $W_R=[\rho_{\mathrm{g}R},\ u_{\mathrm{g}R},\ \rho_{\mathrm{l}R},\ u_{\mathrm{l}R},\ \alpha_{\mathrm{g}R}]^{\mathrm{T}}$.

Across the wave family associated with $\lambda_1=u_{\mathrm{l}}-a_{\mathrm{l}}$ we have

$$\frac{\mathrm{d}\rho_{\mathrm{g}}}{0}=\frac{\mathrm{d}u_{\mathrm{g}}}{0}=\frac{\mathrm{d}\rho_{\mathrm{l}}}{-\rho_{\mathrm{l}}}=\frac{\mathrm{d}u_{\mathrm{l}}}{a_{\mathrm{l}}}=\frac{\mathrm{d}\alpha_{\mathrm{g}}}{0}$$

 

which gives

$$\frac{2a_{\mathrm{l}}}{\gamma_{\mathrm{l}}-1}+u_{\mathrm{l}}=\text{constant} \tag{24}$$

Similarly, across the wave family associated with $\lambda_2=u_{\mathrm{g}}-a_{\mathrm{g}}$ we have

$$\frac{\mathrm{d}\rho_{\mathrm{g}}}{-\rho_{\mathrm{g}}}=\frac{\mathrm{d}u_{\mathrm{g}}}{a_{\mathrm{g}}}=\frac{\mathrm{d}\rho_{\mathrm{l}}}{0}=\frac{\mathrm{d}u_{\mathrm{l}}}{0}=\frac{\mathrm{d}\alpha_{\mathrm{g}}}{0}$$

from which we obtain

$$\frac{2a_{\mathrm{g}}}{\gamma_{\mathrm{g}}-1}+u_{\mathrm{g}}=\text{constant} \tag{25}$$

Analogously, for the wave family associated with $\lambda_4=u_{\mathrm{g}}+a_{\mathrm{g}}$ and $\lambda_5=u_{\mathrm{l}}+a_{\mathrm{l}}$ we, respectively, obtain

$$\frac{2a_{\mathrm{g}}}{\gamma_{\mathrm{g}}-1}-u_{\mathrm{g}}=\text{constant} \tag{26}$$

and

$$\frac{2a_{\mathrm{l}}}{\gamma_{\mathrm{l}}-1}-u_{\mathrm{l}}=\text{constant} \tag{27}$$

For the contact discontinuity associated with $\lambda_3=\lambda$ we obtain the following relations:

$$\begin{aligned}\Delta^*\rho_{\mathrm{g}}&=r_1^{(3)}\Delta\alpha_{\mathrm{g}}\\ \Delta^*u_{\mathrm{g}}&=r_2^{(3)}\Delta\alpha_{\mathrm{g}}\\ \Delta^*\rho_{\mathrm{l}}&=r_3^{(3)}\Delta\alpha_{\mathrm{g}}\\ \Delta^*u_{\mathrm{l}}&=r_4^{(3)}\Delta\alpha_{\mathrm{g}}\end{aligned} \tag{28}$$

where the jumps are

$$\Delta q=q_R-q_L,\quad \Delta^*q=q_R^*-q_L^*$$

with the unknowns $q_k^*$ to be defined.

## 4. AN APPROXIMATE RIEMANN SOLVER

In this section we define the Riemann problem, identify its solution structure and, under the assumption that all non-linear characteristic fields are associated with rarefaction waves, we construct an approximate solution to the Riemann problem. This solution has close form and is exact when, in addition, the jump in volume fractions is trivial.

 

### 4.1. The Riemann problem

Consider the Riemann problem

$$\partial_t W + A(W)\partial_x W = 0$$
$$W(x,0) = \begin{cases} W_L, & x < 0 \\ W_R, & x > 0 \end{cases} \tag{29}$$

where $W$ is the vector of unknowns (14) and the coefficient matrix $A(W)$ is given by (16) with definitions (13). The structure of the solution of (29) is depicted in Figure 1.

There are five wave families associated, respectively, with the eigenvalues $\lambda_1, \ldots, \lambda_5$. There are six constant regions separated by waves, the nature of which is unknown in advance except for the contact discontinuity of speed $\lambda_3 = \lambda$, see Equations (5) and (22). Crucial to finding a solution to (29) is the determination of the two overlapping *star regions* either side of the contact, in which a general unknown is denoted as $q^*$, see Figure 1. The corresponding vectors $W_L^*$ and $W_R^*$ of unknowns are

$$W_L^* = [\rho_{gL}^*,\ u_{gL}^*,\ \rho_{lL}^*,\ u_{lL}^*,\ \alpha_{gL}]^{\mathrm{T}}$$

and

$$W_R^* = [\rho_{gR}^*,\ u_{gR}^*,\ \rho_{lR}^*,\ u_{lR}^*,\ \alpha_{gR}]^{\mathrm{T}}$$

Note that from the eigenstructure analysis we know that $\alpha_g$ only changes (discontinuously) across $\lambda_3 = \lambda$. We thus have eight unknowns in the *star region*.

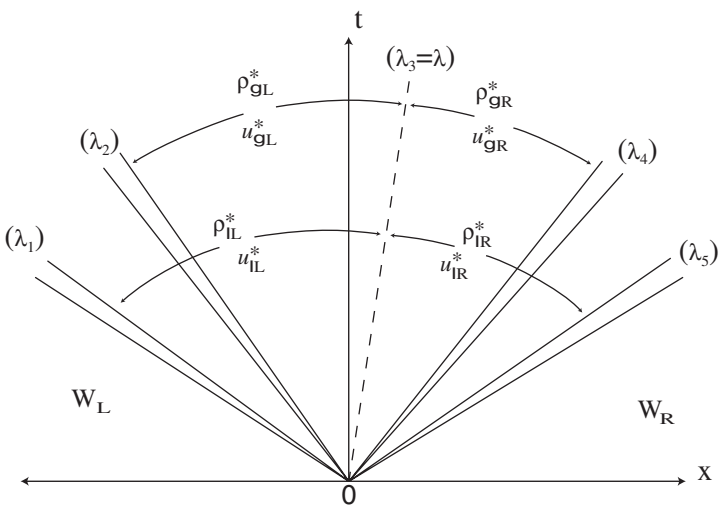


Figure 1. Structure of the solution of the Riemann problem for the two-phase isentropic model of Saurel and Abgrall.

 

### 4.2. *The four-rarefaction approximation*

Here we find an approximate solution by assuming *a priori* that the four outer waves (non-linear) in Figure 1 are rarefaction waves. For this reason the approximation may be called a *Four-rarefaction Riemann solver* and is an extension of the well known two-rarefaction approximation for compressible single phase gas dynamics. Obviously, if all non-linear waves are in fact rarefactions, then the obtained solution is exact. Otherwise, our solution will be an approximation.

For the liquid phase we assume that $W_L$ is connected to $W_L^*$ via the generalized Riemann invariants (GRIs) (24), that is

$$\frac{2a_{lL}^*}{\gamma_l - 1} + u_{lL}^* = \frac{2a_{lL}}{\gamma_l - 1} + u_{lL} \equiv C_{lL} \tag{30}$$

Similarly, the liquid phase in $W_R$ is connected to $W_R^*$ via (27)

$$\frac{2a_{lR}^*}{\gamma_l - 1} - u_{lR}^* = \frac{2a_{lR}}{\gamma_l - 1} - u_{lL} \equiv C_{lR} \tag{31}$$

Analogous relations apply to the gas phase derived from (25) and (26) so that

$$\frac{2a_{gL}^*}{\gamma_g - 1} + u_{gL}^* = \frac{2a_{gL}}{\gamma_g - 1} + u_{gL} \equiv C_{gL} \tag{32}$$

and

$$\frac{2a_{gR}^*}{\gamma_g - 1} - u_{gR}^* = \frac{2a_{gR}}{\gamma_g - 1} - u_{gL} \equiv C_{gR} \tag{33}$$

Across the contact discontinuity associated with $\lambda_3 = \lambda$ relations (28) hold. Considering the relevant relations for the liquid phase we utilize the third and fourth relations of Equations (28), (30) and (31) to obtain a single algebraic non-linear equation for the unknown $\rho_{lL}^* \equiv y$, namely

$$F_l(y) = y^{\gamma_l - 1/2} + [r_3^{(3)}(\alpha_{gR} - \alpha_{gL}) + y]^{\gamma_l - 1/2} - \frac{r_4^{(3)}(\alpha_{gR} - \alpha_{gL}) + C_{lL} + C_{lR}}{C_l} \tag{34}$$

Analogous use of the first and second relations of (28) and Equations (32) and (33) give another non-linear equation for the unknown $\rho_{gL}^* \equiv z$, namely

$$F_g(z) = z^{\gamma_g - 1/2} + [r_1^{(3)}(\alpha_{gR} - \alpha_{gL}) + z]^{\gamma_g - 1/2} - \frac{r_2^{(3)}(\alpha_{gR} - \alpha_{gL}) + C_{gL} + C_{gR}}{C_g} \tag{35}$$

The constant $C_l$ and $C_g$ are defined as

$$C_l \equiv \frac{2\sqrt{K_l \gamma_l / \rho_o^{\gamma_l}}}{\gamma_l - 1}, \quad C_g \equiv \frac{2\sqrt{K_g \gamma_g}}{\gamma_g - 1}$$

 

If the initial data in (29) has $\alpha_{gL} = \alpha_{gR}$ then Equations (34) and (35) readily yield a close form solution for the *star region*

$$\begin{aligned} \rho_l^* &= \left( \frac{C_{lR} + C_{lL}}{2C_l} \right)^{2/\gamma_l - 1} \\ u_l^* &= \frac{C_{lR} - C_{lL}}{2} \\ \rho_g^* &= \left( \frac{C_{gR} + C_{gL}}{2C_g} \right)^{2/\gamma_g - 1} \\ u_g^* &= \frac{C_{gR} - C_{gL}}{2} \end{aligned} \tag{36}$$

We note that in this case there is no jump across the contact discontinuity and $W_L^* = W_R^*$, so that

$$\begin{aligned} \rho_{lL}^* &= \rho_{lR}^* \equiv \rho_l^* \\ u_{lL}^* &= u_{lR}^* \equiv u_l^* \\ \rho_{gL}^* &= \rho_{gR}^* \equiv \rho_g^* \\ u_{gL}^* &= u_{gR}^* \equiv u_g^* \end{aligned} \tag{37}$$

We denote this close form solution by $W_0^* = [\rho_g^*, u_g^*, \rho_l^*, u_l^*, \alpha_g]$.

For the general case $\alpha_{gL} \neq \alpha_{gR}$, in (29) there is a jump across the contact wave and the solution $W_L^*$, $W_R^*$ is found by first finding the roots of (34) and (35) numerically via a Newton–Raphson (NR) method and then use exact wave relations to find the complete solution throughout the wave structure.

Assuming we have computed solutions $y$ and $z$ from (34) and (35), then we have

$$\begin{aligned} \rho_{lL}^* &= y, & \rho_{gL}^* &= z \\ \rho_{lR}^* &= r_3^{(3)}(\alpha_{gR} - \alpha_{gL}) + \rho_{lL}^*, & \rho_{gR}^* &= r_1^{(3)}(\alpha_{gR} - \alpha_{gL}) + \rho_{gL}^* \\ u_{lL}^* &= C_{lL} - C_l \rho_{lL}^{*\,\gamma_l - 1/2}, & u_{gL}^* &= C_{gL} - C_g \rho_{gL}^{*\,\gamma_g - 1/2} \\ u_{lR}^* &= -C_{lR} + C_l \rho_{lR}^{*\,\gamma_l - 1/2}, & u_{gR}^* &= -C_{gR} + C_g \rho_{gR}^{*\,\gamma_g - 1/2} \end{aligned} \tag{38}$$

Note that in (38) the first and third components of the eigenvector $R^{(3)}$ depend on the unknowns of the problem. This leads us to various ways of solving the problem approximately.

### 4.3. Iterative solution

In the presence of a non-trivial contact wave ($\alpha_{gL} \neq \alpha_{gR}$) there will be two distinct regions either side of the contact, that is $W_L^* \neq W_R^*$, see Figure 1.

We have been unable to find a close-form solution for this case. We therefore introduce another level of approximation in order to obtain approximate values for $W_L^*$ and $W_R^*$ by solving iteratively Equations (34) and (35), using as a guess values the closed form solution $W_0^*$ (37). This will be done by a kind of linearization. There are at least two ways of doing this.

 

The simplest linearization is implemented by assuming that $r_1^{(3)}, r_2^{(3)}, r_2^{(3)}, r_4^{(3)}$ in (34) and (35) are constant and are evaluated at the arithmetic means of their arguments using the initial conditions, that is

$$R^{(3)} = R^{(3)}(\tilde{W}) \tag{39}$$

where

$$\tilde{W} = \tfrac{1}{2}(W_L + W_R) \tag{40}$$

Another way is to start with

$$R_0^{(3)} = R_0^{(3)}(W_0^*) \tag{41}$$

where $W_0^*$ is given by (37). For iteration $k+1$ we set

$$R_k^{(3)} = R_k^{(3)}(W_k^*) \tag{42}$$

where $W_k^*$ is an arithmetic mean of $W_L^*$ and $W_R^*$ obtained at the $k$th Newton–Raphson iteration.

There is some flexibility in this approach, as the vector $R_k^{(3)}$ could be frozen for the remaining iterations, saving computational time in this manner.

### 4.4. Typical theoretical solutions

In what follows we consider some specific examples, for which the initial conditions are given in Tables I–IV.

Table I. Initial conditions for Test 1.

| | | | | | |
|---|---|---|---|---|---|
| $W_L$ | $\rho_{gL}$ | $u_{gL}$ | $\rho_{lL}$ | $u_{lL}$ | $\alpha_{gL}$ |
| | 719.6856 | −350 | 1225.8912 | −350 | 0.9 |
| $W_R$ | $\rho_{gR}$ | $u_{gR}$ | $\rho_{lR}$ | $u_{lR}$ | $\alpha_{gR}$ |
| | 719.6856 | 350 | 1225.8912 | 350 | 0.9 |

Table II. Initial conditions for Test 2.

| | | | | | |
|---|---|---|---|---|---|
| $W_L$ | $\rho_{gL}$ | $u_{gL}$ | $\rho_{lL}$ | $u_{lL}$ | $\alpha_{gL}$ |
| | 719.6856 | −350 | 1225.8912 | −250 | 0.9 |
| $W_R$ | $\rho_{gR}$ | $u_{gR}$ | $\rho_{lR}$ | $u_{lR}$ | $\alpha_{gR}$ |
| | 719.6856 | 350 | 1225.8912 | 250 | 0.1 |

Table III. Initial conditions for Test 3.

| | | | | | |
|---|---|---|---|---|---|
| $W_L$ | $\rho_{gL}$ | $u_{gL}$ | $\rho_{lL}$ | $u_{lL}$ | $\alpha_{gL}$ |
| | 719.6856 | 150 | 1225.8912 | 150 | 0.9 |
| $W_R$ | $\rho_{gR}$ | $u_{gR}$ | $\rho_{lR}$ | $u_{lR}$ | $\alpha_{gR}$ |
| | 719.6856 | −150 | 1225.8912 | −150 | 0.9 |

 

Table IV. Initial conditions for Test 4.

| | | | | | |
|---|---|---|---|---|---|
| $W_L$ | $\rho_{gL}$ | $u_{gL}$ | $\rho_{lL}$ | $u_{lL}$ | $\alpha_{gL}$ |
| | 719.6856 | 1000.00 | 1225.8912 | 2400.00 | 0.9 |
| $W_R$ | $\rho_{gR}$ | $u_{gR}$ | $\rho_{lR}$ | $u_{lR}$ | $\alpha_{gR}$ |
| | 261.5970 | 2277.81 | 1028.3588 | 2774.36 | 0.9 |

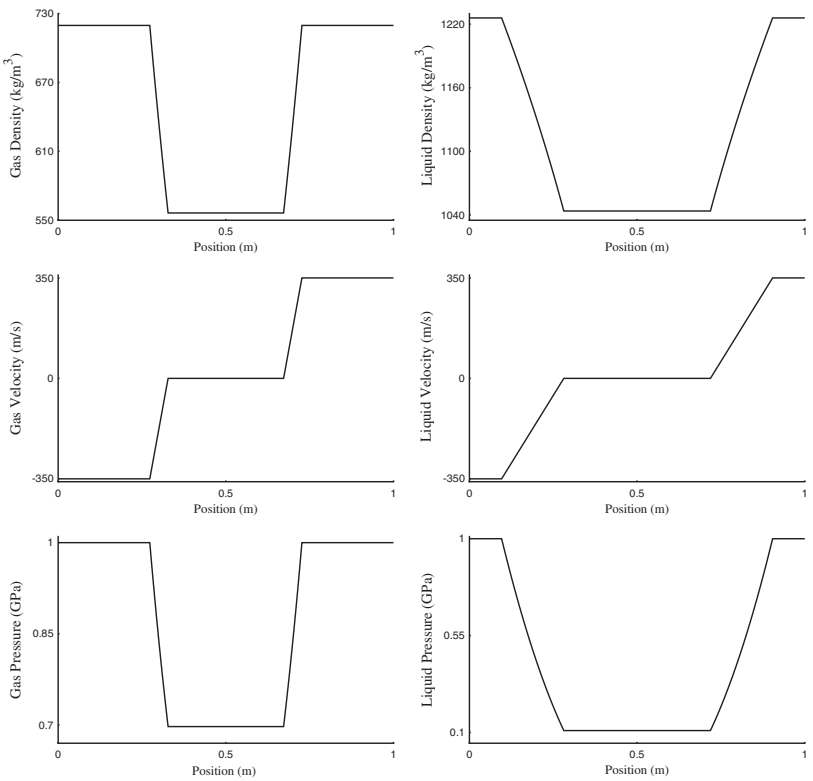


Figure 2. Exact solution profiles for Test 1.

In Test 1 the exact solution consists on four symmetric rarefaction waves and a trivial contact discontinuity, that is $\alpha_L = \alpha_R$. For this case our theoretical solution (37) is exact. See Figure 2. Test 2 consists of four rarefaction waves and a non-trivial contact discontinuity. For this example our theoretical solution is iterative and is only an approximation to the exact solution, which is unknown to us. See Figure 3. Test 3 consists of four symmetric shock waves (weak) and a trivial contact discontinuity. For this case our theoretical solution can only be regarded as a crude approximation to the exact solution. First we remark that the theoretical correctness of shock wave solutions for non-conservative hyperbolic systems is currently unknown. Our theoretical approximation is based on the *star values* obtained from the four-rarefaction assumption and then we have estimated the shock speeds as an

 

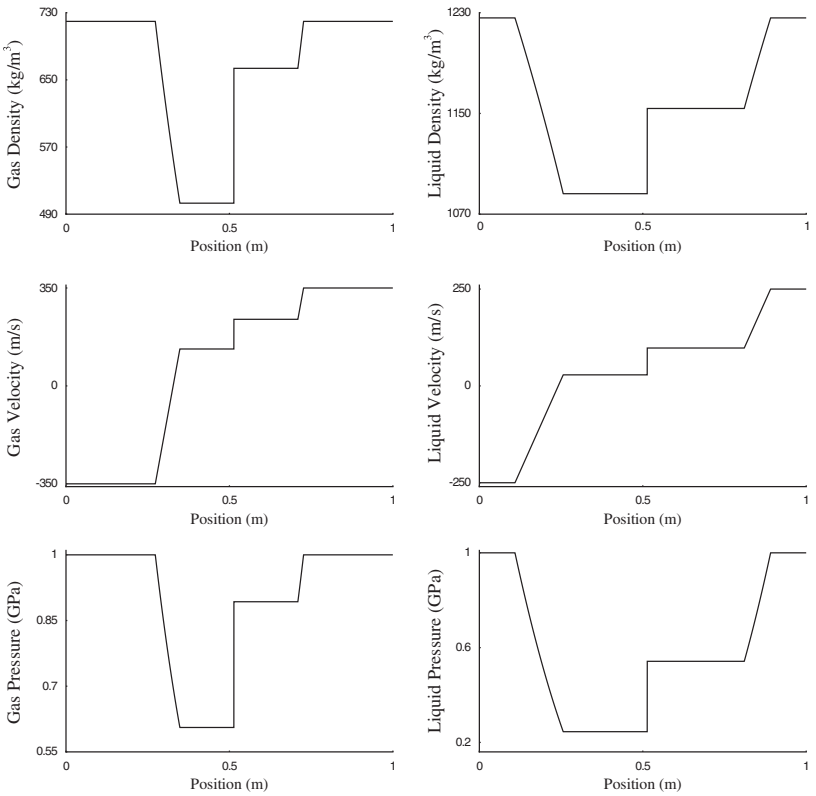


Figure 3. Approximate solution profiles for Test 2.

arithmetic mean of the characteristic speeds ahead and behind of the shock. It is surprising that this theoretical solution appears to be accurate, as verified by independent numerical calculations. See also Figure 11. Test 4 consists of a single rarefaction wave for each phase. See Figure 14. The point of having chosen this test, for which our theoretical solution (37) is exact, is that it contains a *sonic point*, for which numerical methods tend to encounter difficulties.

In Section 5 we utilize the theoretical solution just described, locally, to construct upwind methods, and in Section 6 we utilize these theoretical solutions to assess the performance of numerical methods.

In order to test the sensitivity of the NR iteration process we solved (34), (35) for the case $\alpha_{gL} = \alpha_{gR}$, which has closed form solution $W_0^*$ (37). We perform numerical experiments for a variety of guess values. Table V shows the iterative process with a guess value given by $W_L$. Using a tolerance $\mathrm{TOL} = 10^{-10}$ we needed five iterations to reach the exact solution. This assure us that the NR solver works as expected.

Tables VI and VII show the results of the iterative process for Test 2, see Table II. With initial guess $W_0^*$ of Equations (37) and $\mathrm{TOL} = 10^{-10}$ one requires 17 iterations to achieve

 

Table V. Newton–Rhapson iterative method for Test 1 using $W_0^*$ and $W_L$ as guess values.

| Guess | Iterations | $\rho_{gL}^*$ | $\rho_{lL}^*$ |
|---|---|---|---|
| $W_0^*$ | 0 | 556.326373426819 | 1043.712366756080 |
| $W_L$ | 0 | 719.685673001152 | 1225.891245955086 |
| | 1 | 539.085437528560 | 1070.309619769666 |
| | 2 | 556.109954607825 | 1044.391992046297 |
| | 3 | 556.326339745587 | 1043.712825491585 |
| | 4 | 556.326373426818 | 1043.712366756289 |
| | 5 | 556.326373426819 | 1043.712366756080 |

Table VI. Newton–Rhapson iterative method for Test 2 with initial guess $W_0^*$.

| Guess | Iterations | $\rho_{gL}$ | $\rho_{lL}$ |
|---|---|---|---|
| $W_0^*$ | 0 | 556.326373426819 | 1102.300274722990 |
| | 1 | 467.936108470893 | 1062.762255129332 |
| | 2 | 499.143312440224 | 1082.603301710746 |
| | 3 | 505.307421321565 | 1087.953568950437 |
| | 4 | 503.085390407153 | 1086.268154757242 |
| | 5 | 502.893359547870 | 1086.101145817396 |
| | 6 | 503.090428017176 | 1086.255866150020 |
| | 7 | 503.099999842434 | 1086.264388588076 |
| | 8 | 503.083373932929 | 1086.251378688327 |
| | 9 | 503.083241771857 | 1086.251181838734 |
| | 10 | 503.084617230534 | 1086.252262815385 |
| | 11 | 503.084574708412 | 1086.252236969768 |
| | 12 | 503.084462991198 | 1086.252148885975 |
| | 13 | 503.084470840452 | 1086.252154440846 |
| | 14 | 503.084479743406 | 1086.252161485132 |
| | 15 | 503.084478750262 | 1086.252160753366 |
| | 16 | 503.084478055064 | 1086.252160201203 |
| | 17 | 503.084478163955 | 1086.252160282988 |

convergence. We note that other choices of initial guess, such a $W_L$, or $W_R$ do not significantly increase the number of iterations required for convergence, see Table VII.

We also note that for numerical purposes when computing a numerical flux the approximate solution obtained after a couple of iterations is sufficiently accurate, in particular in the numerical results presented in Section 6 the solution obtained with the tolerance $\mathrm{TOL} = 10^{-6}$ was sufficiently good.

### *4.5. The complete solution*

In the previous subsections we have obtained exact and approximate solutions for quantities in the *star region*. The solution in the rest of the half plane of Figure 1 is obtained by applying exact waves relations. Figure 2 shows the exact solution profiles for liquid and gas

 

Table VII. Newton–Rhapson iterative method for Test 2 with initial guess $W_L$.

| Guess | Iterations | $\rho_{gL}$ | $\rho_{lL}$ |
|---|---|---|---|
| $W_L$ | 0 | 719.685673001152 | 1225.891245955086 |
| | 1 | 539.085437528560 | 1114.761512965500 |
| | 2 | 486.563771816759 | 1073.835523325850 |
| | 3 | 495.183975812781 | 1079.136911483718 |
| | 4 | 503.448703767244 | 1086.620103549050 |
| | 5 | 503.728042713983 | 1086.742797532298 |
| | 6 | 503.008799654429 | 1086.197895861312 |
| | 7 | 503.034388137897 | 1086.212178969972 |
| | 8 | 503.092541654627 | 1086.258239352428 |
| | 9 | 503.088292276292 | 1086.255202696258 |
| | 10 | 503.083664516826 | 1086.251541657698 |
| | 11 | 503.084195457077 | 1086.251933468607 |
| | 12 | 503.084556260240 | 1086.252220133637 |
| | 13 | 503.084498472983 | 1086.252176685260 |
| | 14 | 503.084470981336 | 1086.252154747722 |
| | 15 | 503.084476813385 | 1086.252159181866 |
| | 16 | 503.084478852580 | 1086.252160817633 |
| | 17 | 503.084478292589 | 1086.252160388548 |
| | 18 | 503.084478146285 | 1086.252160270407 |

variables at a given output time of $1.3 \times 10^{-4}$ s. For this example the assumption that the four nonlinear waves are rarefaction waves is correct and the further assumption $\alpha_L = \alpha_R$ (trivial contact) allows us to find the analytical solution displayed in Figure 2.

In Figure 3 we display the complete approximate solution to Test 3. Again, the solution consist of four rarefaction waves, as correctly assumed in the approximation scheme. However, given the fact that $\alpha_L \neq \alpha_R$, we must employ an iterative procedure to find numerical values for the variables in the *star regions*.

The theoretical solution obtained in this section can be used for validating numerical computations for the two phase flow model (1)–(5). Moreover, we shall use the relevant information available from the theoretical solution to implement upwind numerical methods to solve the general initial-boundary value problem for Equations (1)–(5). This is the subject of the next section.

## 5. CONSTRUCTION OF UPWIND NUMERICAL METHODS

In this section we construct upwind numerical methods for solving the complete initial-boundary value problem for Equations (1)–(5) in the non-conservative forms (10) or (15). The schemes presented make use of the approximate Riemann solver of Section 4. One of the methods is the non-conservative analogue of the Godunov first-order upwind method. The other methods considered are second-order accurate in space and time and are non-linear (non-oscillatory), using total variation diminishing (TVD) and essentially non-oscillatory (ENO) criteria to control spurious oscillations near large gradients of the solution.

 

The non-conservative schemes are constructed on the basis of an extension of the finite volume approach to non-conservative systems [14, 15]. The schemes have the form

$$W_i^{n+1} = W_i^n - \frac{\Delta t}{\Delta x} \hat{A}_i [W_{i+1/2} - W_{i-1/2}] \tag{43}$$

where $W_i^n$ is a spatial integral average within *volume*, *or cell*, $i$ of length $\Delta x$, at time level $n$; the coefficient matrix $\hat{A}_i$ is an approximation to a space–time integral of the coefficient matrix of the relevant quasi-linear system within volume $i$; $W_{i+1/2}$ is an *intercell state*, analogous to the intercell flux in conservative methods; $\Delta t$ is the time step, computed from a stability condition, which for the methods presented here is $0 < C_{\text{cfl}} \leqslant 1$, where $C_{\text{cfl}}$ is the usual CFL or Courant number coefficient. The second-order schemes are: an ADER second-order scheme and the MUSCL_Hancock scheme.

### 5.1. A second-order ADER scheme

To construct a second-order ADER scheme [16], we assume a piece-linear reconstruction and consider the piecewise linear Riemann problem

$$\begin{gathered} \partial_t W + A(W)\partial_x W = 0 \\ W(x,0) = \begin{cases} W_L(x) \equiv W_i^n + \dfrac{(x - x_i)}{\Delta x} \Delta_i \\ W_R(x) \equiv W_{i+1}^n + \dfrac{(x - x_{i+1})}{\Delta x} \Delta_{i+1} \end{cases} \end{gathered} \tag{44}$$

The solution of this *derivative Riemann problem* at the interface is expressed as

$$W_{i+1/2}(\tau) = W_{i+1/2}^{(0)}(0) + \tau \partial_t W_{i+1/2}(0) \tag{45}$$

The leading term is evaluated from the solution of the piecewise constant Riemann problem with initial data consisting of the boundary extrapolated values from (44). To compute the second-term we use the Cauchy–Kowalewski method and express time derivatives in terms of space derivatives. For example, from Equation (15) we write

$$\partial_t W = -A(W)\partial_x W \tag{46}$$

and is replaced in Equation (45) obtaining

$$W_{i+1/2}(\tau) = W_{i+1/2}^{(0)}(0) - \tau \; A(W_{i+1/2}^{(0)}(0))\partial_x W_{i+1/2}(0) \tag{47}$$

 

The vector $V \equiv \partial_x W$ obeys the linear homogeneous evolution equation

$$\partial_t V + \hat{A}\partial_x V = 0 \tag{48}$$

To find $V$ at the interface $x_{i+1/2}$ we solve the linearized Riemann problem

$$\partial_t V + \hat{A}\ \partial_x V = 0$$
$$V(x,0) = \begin{cases} V_L \equiv \partial_x W_L \\ V_R \equiv \partial_x W_R \end{cases} \tag{49}$$

The exact solution to this problem is standard

$$\partial_x W(0) = V_L + \sum_{\lambda_k \leqslant 0} \alpha_k R^{(k)} \tag{50}$$

where $R^{(k)}$ are the right eigenvectors of $\hat{A}_{i+1/2}$, $\alpha_k$ are the wave strengths and $\lambda_k$ are the eigenvalues of $\hat{A}_{i+1/2}$. The matrix is taken as

$$\hat{A}_{i+1/2} = A(W^{(0)}_{i+1/2}(0)) \tag{51}$$

leading to a solution $W^{(1)}_{i+1/2}(0) = \partial_x W(0)$ and finally we have

$$W_{i+1/2}(\tau) = W^{(0)}_{i+1/2}(0) - \tau A(W^{(0)}_{i+1/2}(0))\ W^{(1)}_{i+1/2}(0) \tag{52}$$

From this, the intercell state is obtained by taking the integral average

$$W_{i+1/2} = \frac{1}{\Delta t}\int_0^{\Delta t} (W^{(0)}_{i+1/2}(0) - \tau A(W^{(0)}_{i+1/2}(0))\ W^{(1)}_{i+1/2}(0))\,\mathrm{d}t$$

which integrates exactly to give

$$W_{i+1/2} = W^{(0)}_{i+1/2}(0) - \frac{\Delta t}{2}\ A(W^{(0)}_{i+1/2}(0))\ W^{(1)}_{i+1/2}(0) \tag{53}$$

which is the ADER interface state to be used in formula (43), where the coefficient matrix is taken as

$$\hat{A}_i = A\left(\frac{1}{2}(W_{i-1/2} + W_{i+1/2})\right) \tag{54}$$

### *5.2. The MUSCL_Hancock method*

In this approach [17] data reconstruction is performed using piecewise linear functions, see (44), and boundary extrapolated values are evolved by half a time step and then used as initial data for a piecewise constant Riemann problem. Non-oscillatory properties come from TVD slope limiters in the data reconstruction. See Reference [8] for more details.

 

The piecewise linear reconstruction has boundary extrapolated values

$$W_i^L = W_i^n - \tfrac{1}{2}\Delta_i, \quad W_i^R = W_i^n + \tfrac{1}{2}\Delta_i \tag{55}$$

where

$$\Delta_i = \tfrac{1}{2}(1+\omega)\Delta_{i-1/2} + \tfrac{1}{2}(1-\omega)\Delta_{i+1/2}, \quad \Delta_{i-1/2} = W_i - W_{i-1}, \ \ \Delta_{i+1/2} = W_{i+1} - W_i$$

with $\omega \in [-1, 1]$. The boundary extrapolated values (55) are evolved thus

$$\bar{W}_i^L = W_i^L + \frac{1}{2}\frac{\Delta t}{\Delta x}\tilde{A}_i[W_i^L - W_i^R], \quad \bar{W}_i^R = W_i^R + \frac{1}{2}\frac{\Delta t}{\Delta x}\tilde{A}_i[W_i^L - W_i^R]$$

leading to the expressions

$$\bar{W}_i^L = W_i^n - \frac{1}{2}\left[\mathrm{I} + \frac{\Delta t}{\Delta x}\tilde{A}_i\right]\Delta_i, \quad \bar{W}_i^R = W_i^n + \frac{1}{2}\left[\mathrm{I} - \frac{\Delta t}{\Delta x}\tilde{A}_i\right]\Delta_i \tag{56}$$

where the coefficient matrix is taken as $\tilde{A}_i = A(W_i^n)$.

To compute the intercell state at $x_{i+1/2}$ we utilize $\bar{W}_i^R$ and $\bar{W}_{i+1}^L$ as the initial data for a conventional piecewise constant Riemann problem, leading to the sought solution $W_{i+1/2}$, which is then utilized in the update formula (43); the coefficient matrix of which has the same form as for the ADER method, see (54).

A remark is in order, regarding the choice of the coefficient matrices in, for example (43), (52) and (53). Since we are dealing with non-conservative systems and non-conservative methods there is an uncertainty as to the correct solution for shocks. The choice of the coefficient matrix could be a factor in determining shock solutions.

## 6. NUMERICAL RESULTS

The proposed numerical methods are assessed via a number of test problems for which we can also use the theoretical solutions of this paper to compare with. We consider the four test problems introduced in Section 4.4, solved on a spatial domain $[0, 1]$, and the initial conditions of which are given in Tables I–IV. The structure of the exact solution for each of the test problems is described in Section 4.4. For Tests 1–3 the initial discontinuity in flow variable is positioned at $x = 0.5$ and solutions are displayed at time $t_{\text{out}} = 1.3 \times 10^{-4}$ s. For the sonic flow problem, Test 4, the initial discontinuity is positioned at $x = 0.3$ and the solution is displayed at time $t_{\text{out}} = 4.0 \times 10^{-4}$ s. The constant used in the equations of state (8) and (9) are: $K_{\text{g}} = 1 \times 10^5$ Pa, $\gamma_{\text{g}} = 1.4$, $K_{\text{l}} = 3.03975 \times 10^8$ Pa, $\gamma_{\text{l}} = 7.15$, $\rho_o = 1 \times 10^3$ kg/m$^3$.

Numerical results are compared with theoretical solutions in Figures 4–16. The CFL coefficient used for each computation is displayed in each of the results. We use the SUPERBEE limiter for the MUSCL_Hancock, whereas for ADER we use piecewise linear ENO reconstructions.

In the computations we have used the following meshes: $M = 100$, 200 and 800. The first mesh allows us to asses the performance of the method for realistically coarse meshes. The second mesh allows us to asses the convergence trend of the numerical solutions and the last mesh allows us to verify that the converged numerical solution is close to the theoretical solution.

 

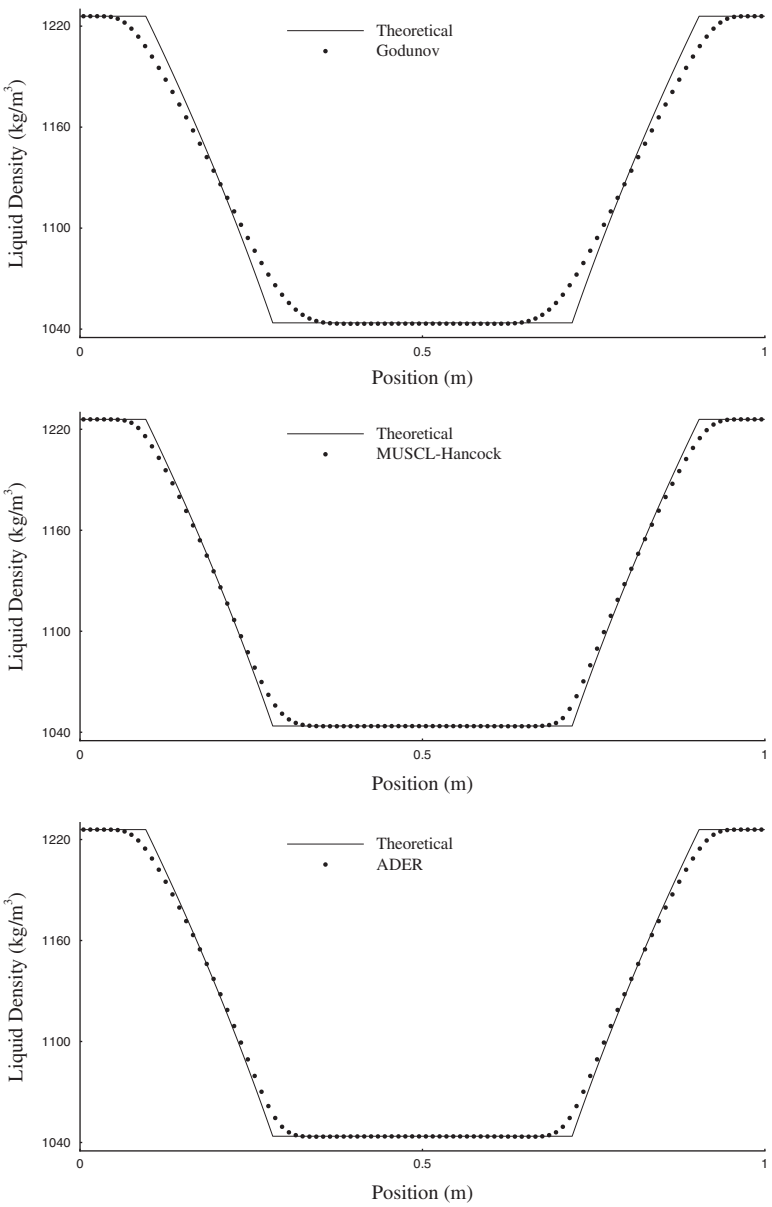


Figure 4. TEST 1: Numerical results for liquid density (symbols) from three numerical methods (Godunov, MUSCL_Hancock and ADER) are compared with the theoretical solution (line). CFL coefficient used is $C_{\text{cfl}} = 0.9$ and mesh used is $M = 100$ cells.

 

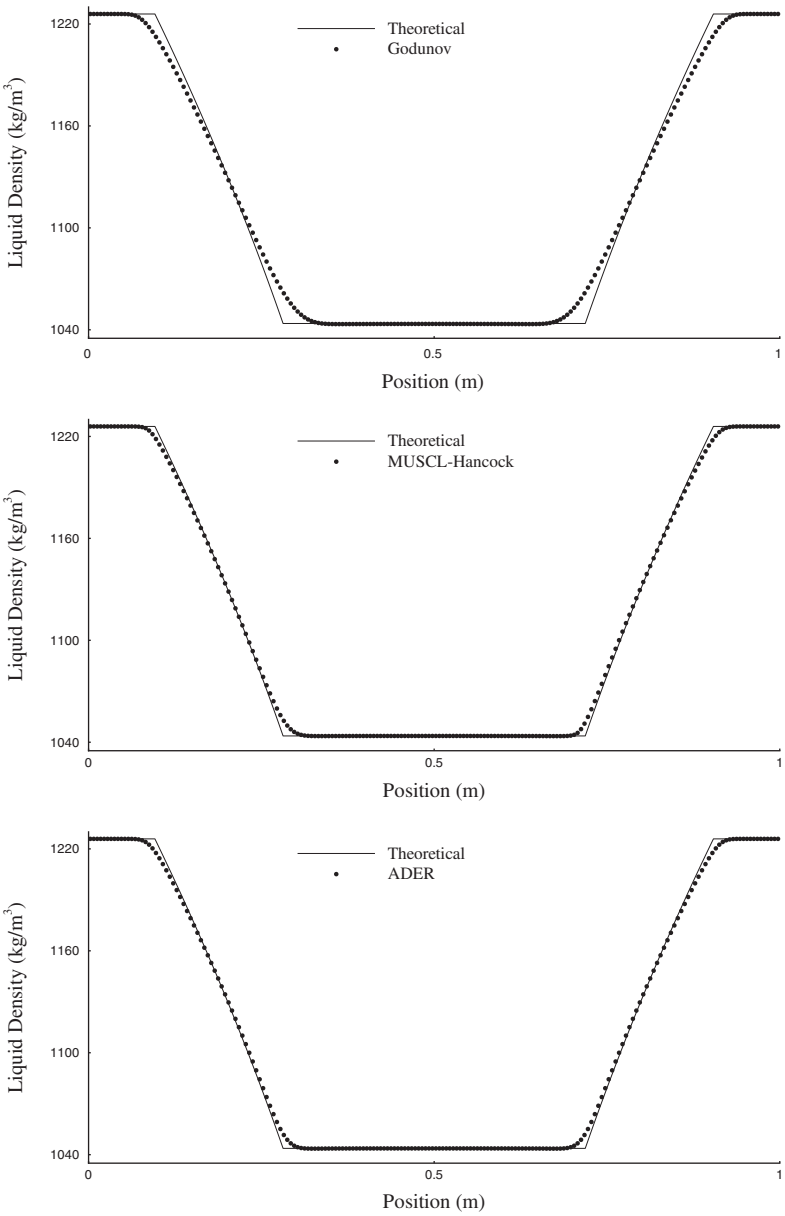


Figure 5. TEST 1: Numerical results for liquid density (symbols) from three numerical methods (Godunov, MUSCL_Hancock and ADER) are compared with the theoretical solution (line). CFL coefficient used is $C_{\mathrm{cfl}} = 0.9$ and mesh used is $M = 200$ cells.

 

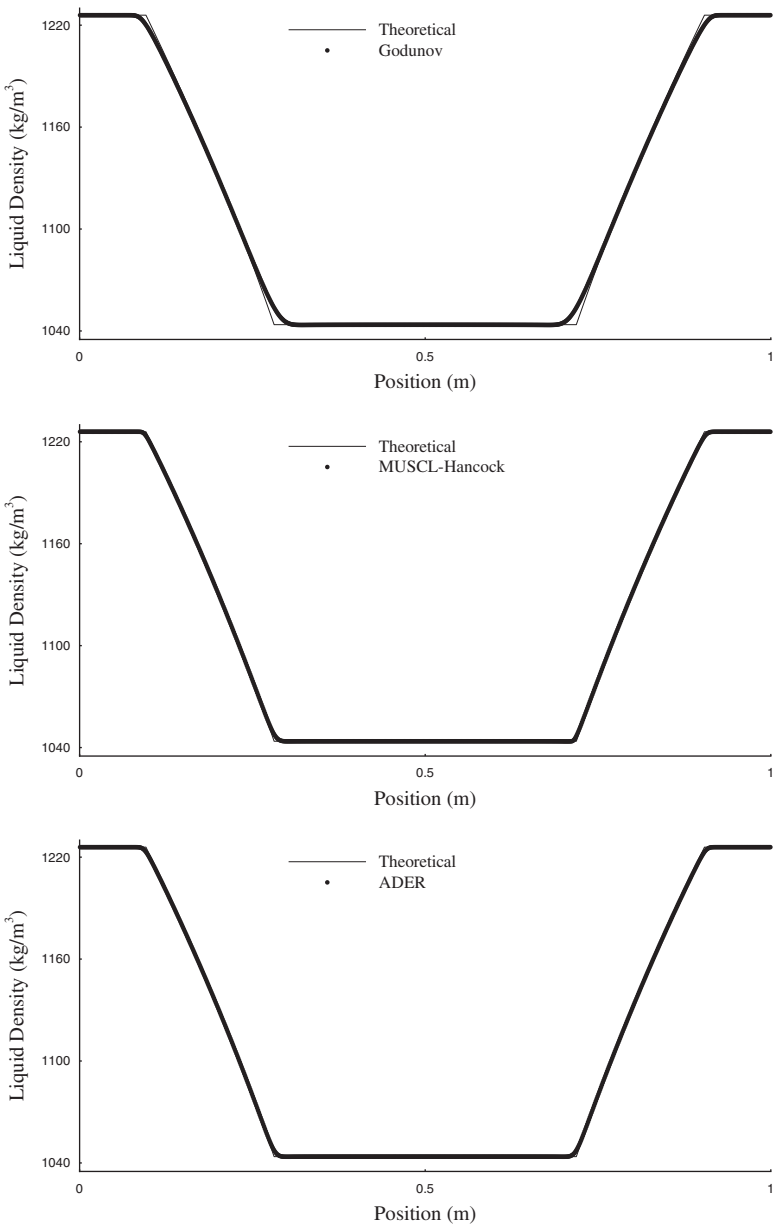


Figure 6. TEST 1: Numerical results for liquid density (symbols) from three numerical methods (Godunov, MUSCL_Hancock and ADER) are compared with the theoretical solution (line). CFL coefficient used is $C_{\text{cfl}} = 0.9$ and mesh used is $M = 800$ cells.

 

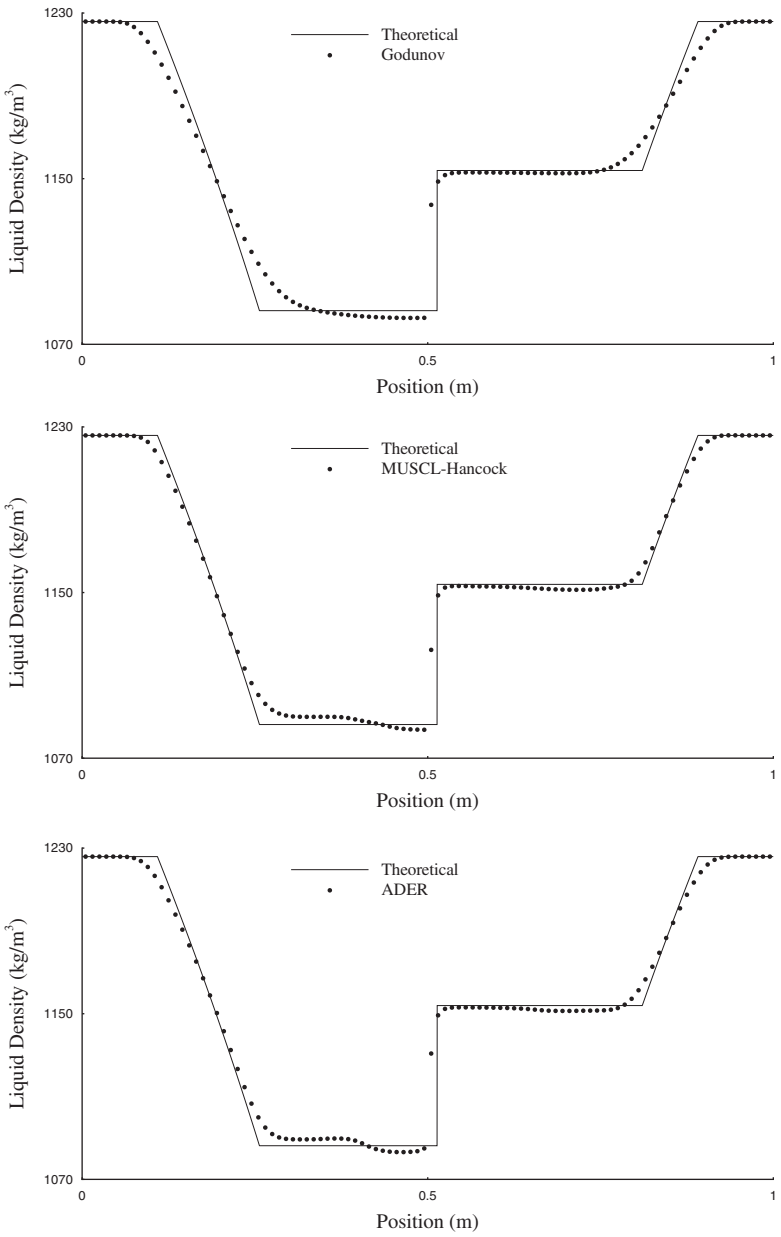


Figure 7. TEST 2: Numerical results for liquid density (symbols) from three numerical methods (Godunov, MUSCL_Hancock and ADER) are compared with the theoretical solution (line). CFL coefficient used is $C_{\mathrm{cfl}} = 0.9$ and mesh used is $M = 100$ cells.

 

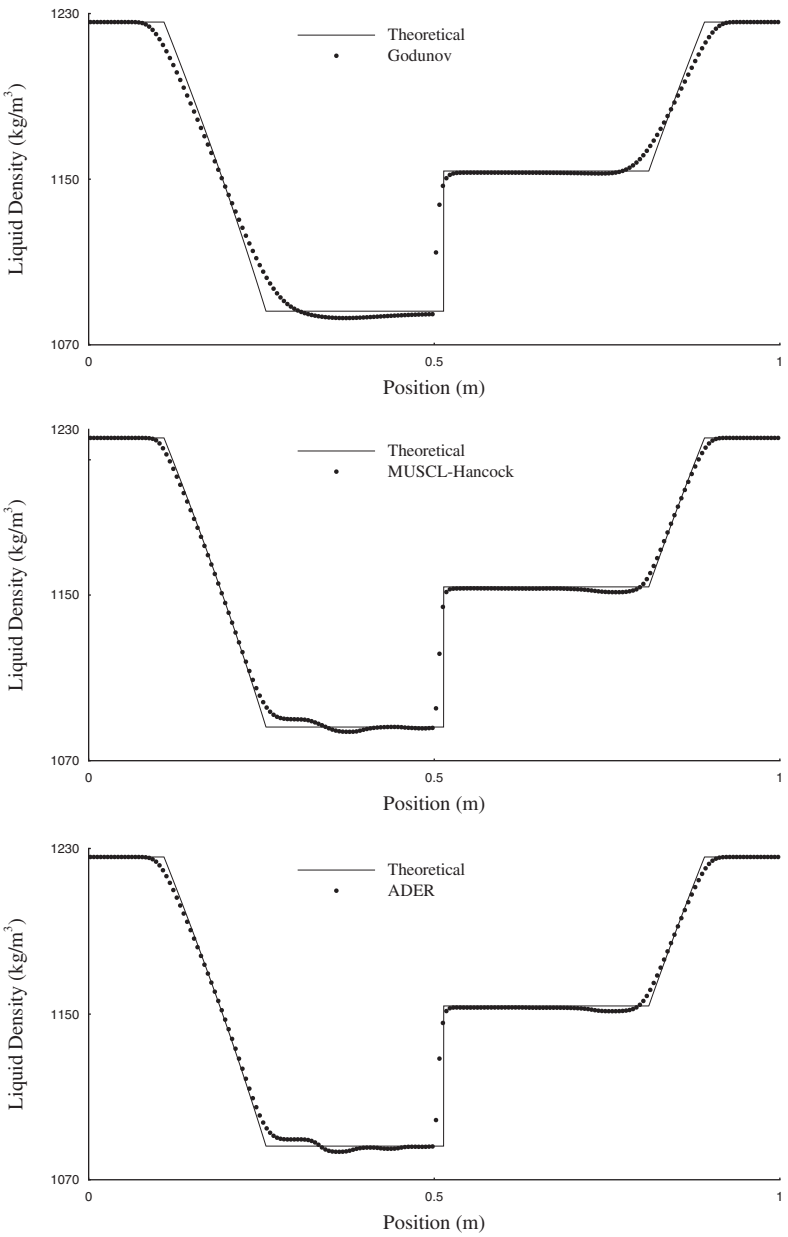


Figure 8. TEST 2: Numerical results for liquid density (symbols) from three numerical methods (Godunov, MUSCL_Hancock and ADER) are compared with the theoretical solution (line). CFL coefficient used is $C_{\mathrm{cfl}} = 0.9$ and mesh used is $M = 200$ cells.

 

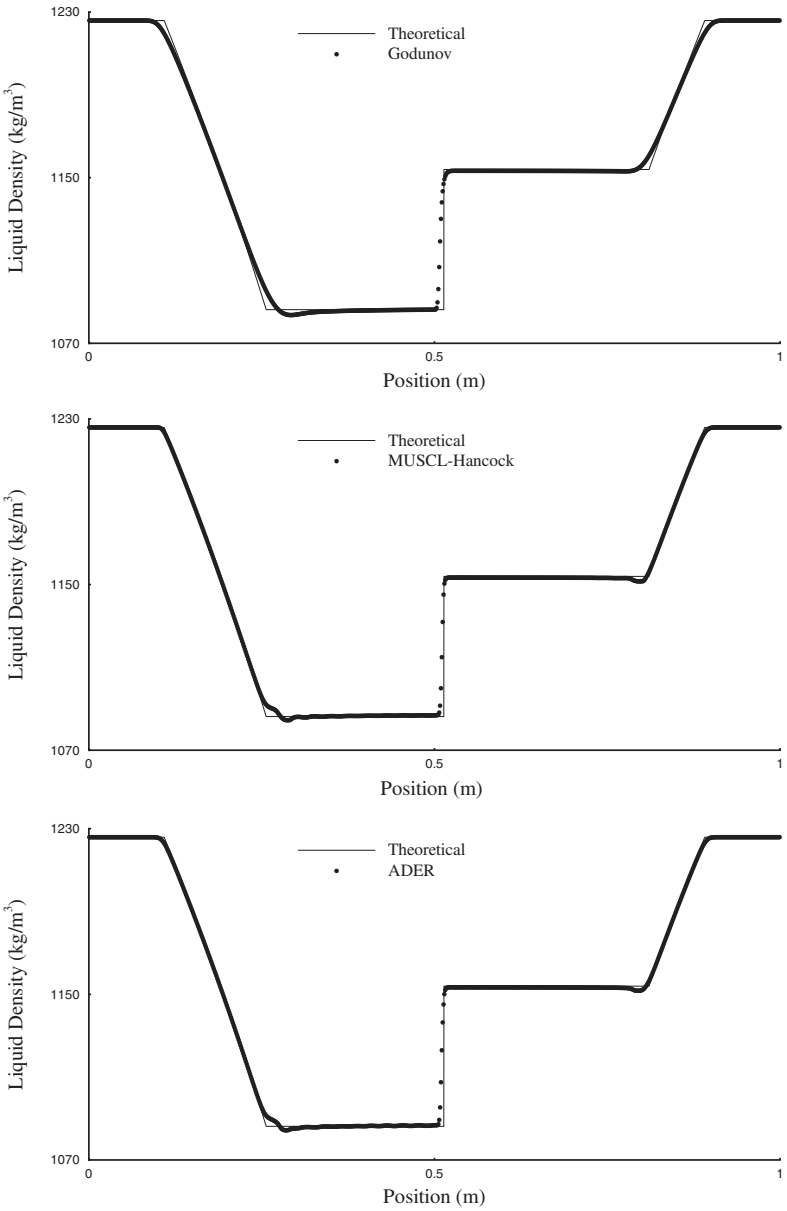


Figure 9. TEST 2: Numerical results for liquid density (symbols) from three numerical methods (Godunov, MUSCL_Hancock and ADER) are compared with the theoretical solution (line). CFL coefficient used is $C_{\mathrm{cfl}} = 0.9$ and mesh used is $M = 800$ cells.

 

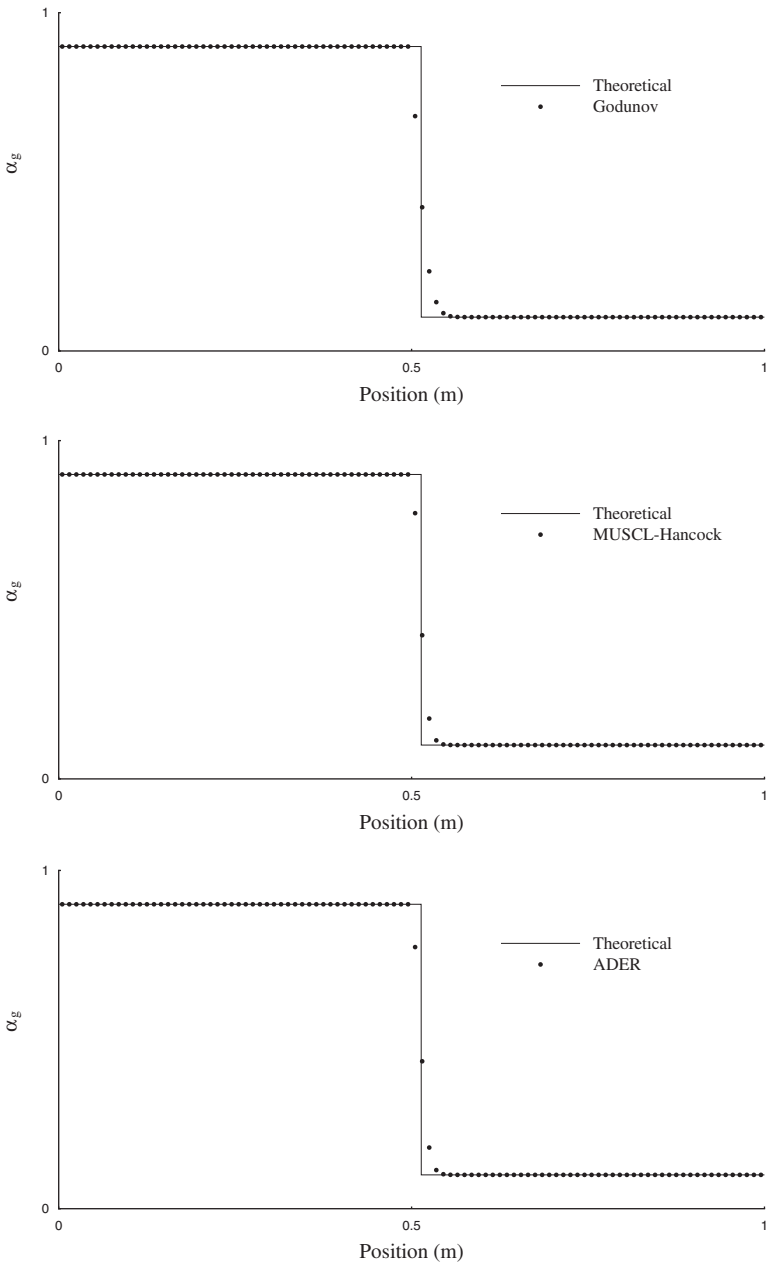


Figure 10. TEST 2: Numerical results for gas volume fraction (symbols) from three numerical methods (Godunov, MUSCL_Hancock and ADER) are compared with the theoretical solution (line). CFL coefficient used is $C_{\text{cfl}} = 0.9$ and mesh used is $M = 100$ cells.

 

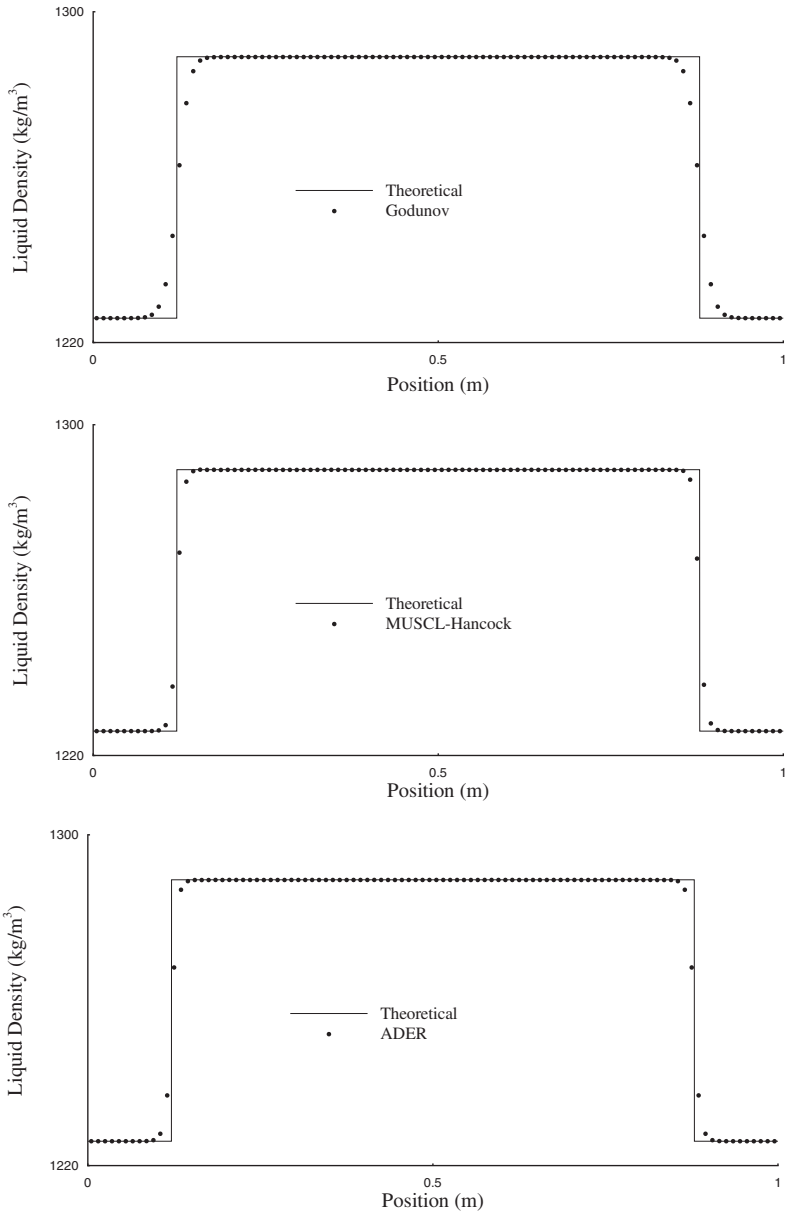


Figure 11. TEST 3: Numerical results for liquid density (symbols) from three numerical methods (Godunov, MUSCL_Hancock and ADER) are compared with the theoretical solution (line). CFL coefficient used is $C_{\text{cfl}} = 0.9$ and mesh used is $M = 100$ cells.

 

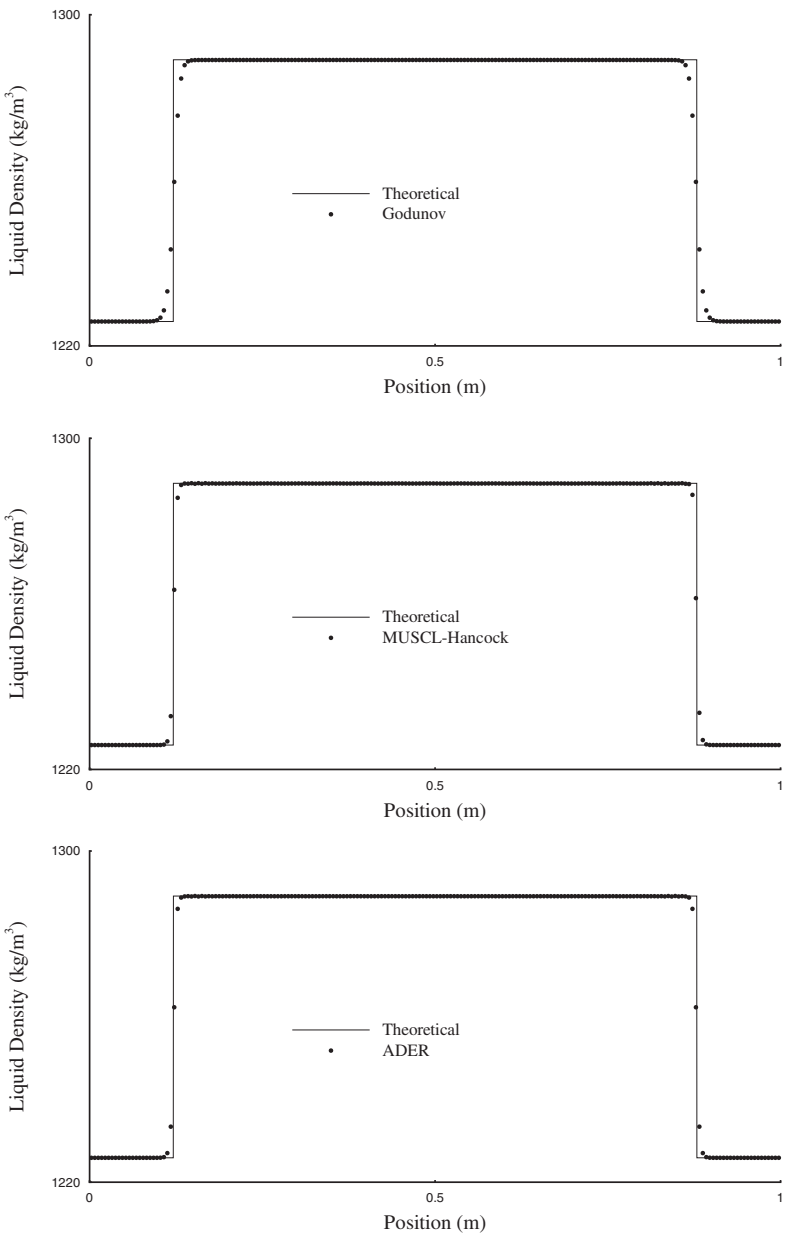


Figure 12. TEST 3: Numerical results for liquid density (symbols) from three numerical methods (Godunov, MUSCL_Hancock and ADER) are compared with the theoretical solution (line). CFL coefficient used is $C_{\text{cfl}} = 0.9$ and mesh used is $M = 200$ cells.

 

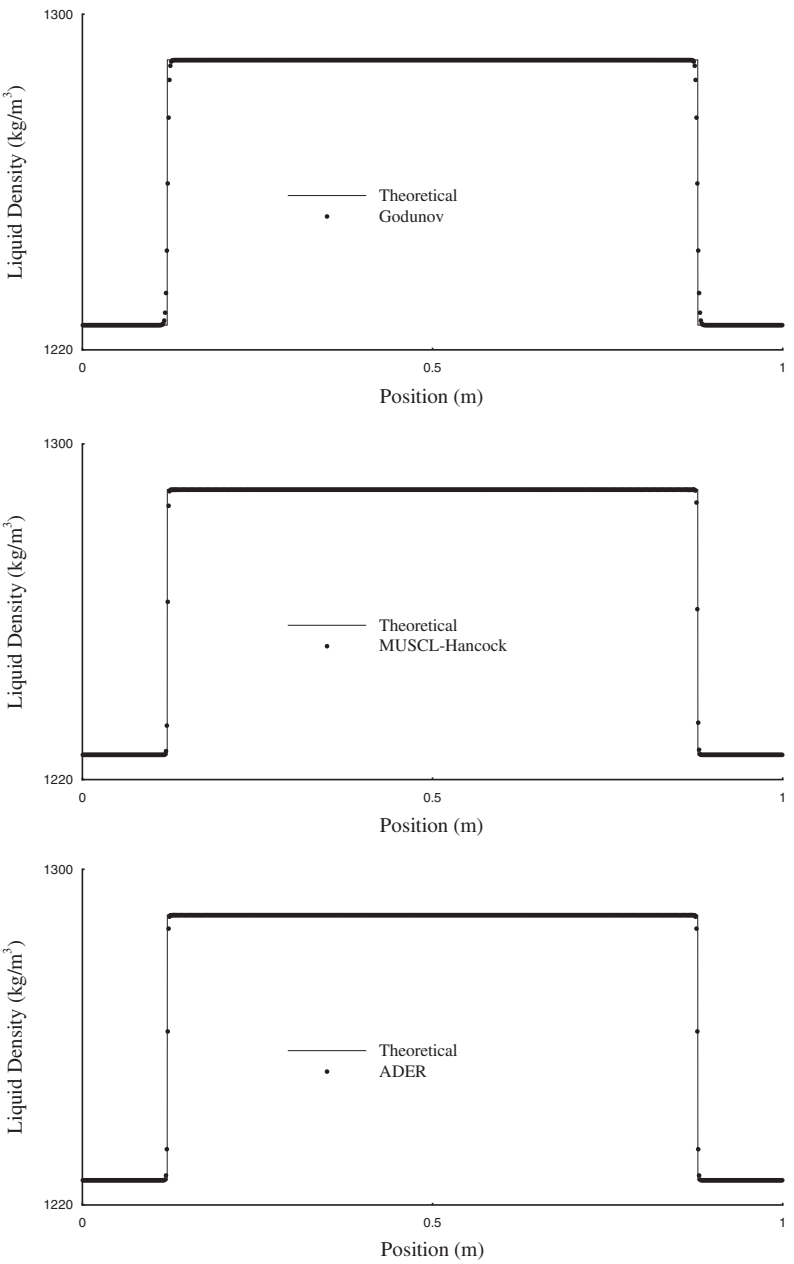


Figure 13. TEST 3: Numerical results for liquid density (symbols) from three numerical methods (Godunov, MUSCL_Hancock and ADER) are compared with the theoretical solution (line). CFL coefficient used is $C_{\mathrm{cfl}} = 0.9$ and mesh used is $M = 800$ cells.

 

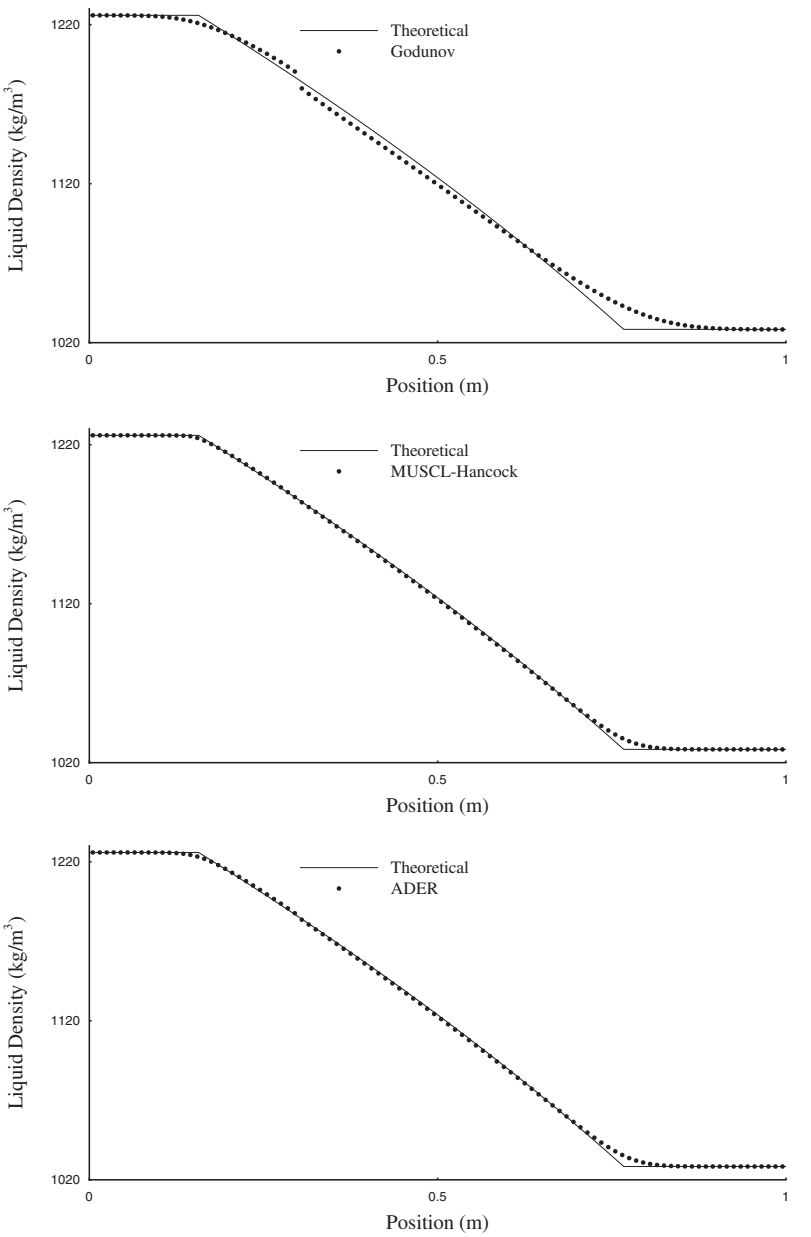


Figure 14. TEST 4: Numerical results for liquid density (symbols) from three numerical methods (Godunov, MUSCL_Hancock and ADER) are compared with the theoretical solution (line). CFL coefficient used is $C_{\text{cfl}} = 0.9$ and mesh used is $M = 100$ cells.

 

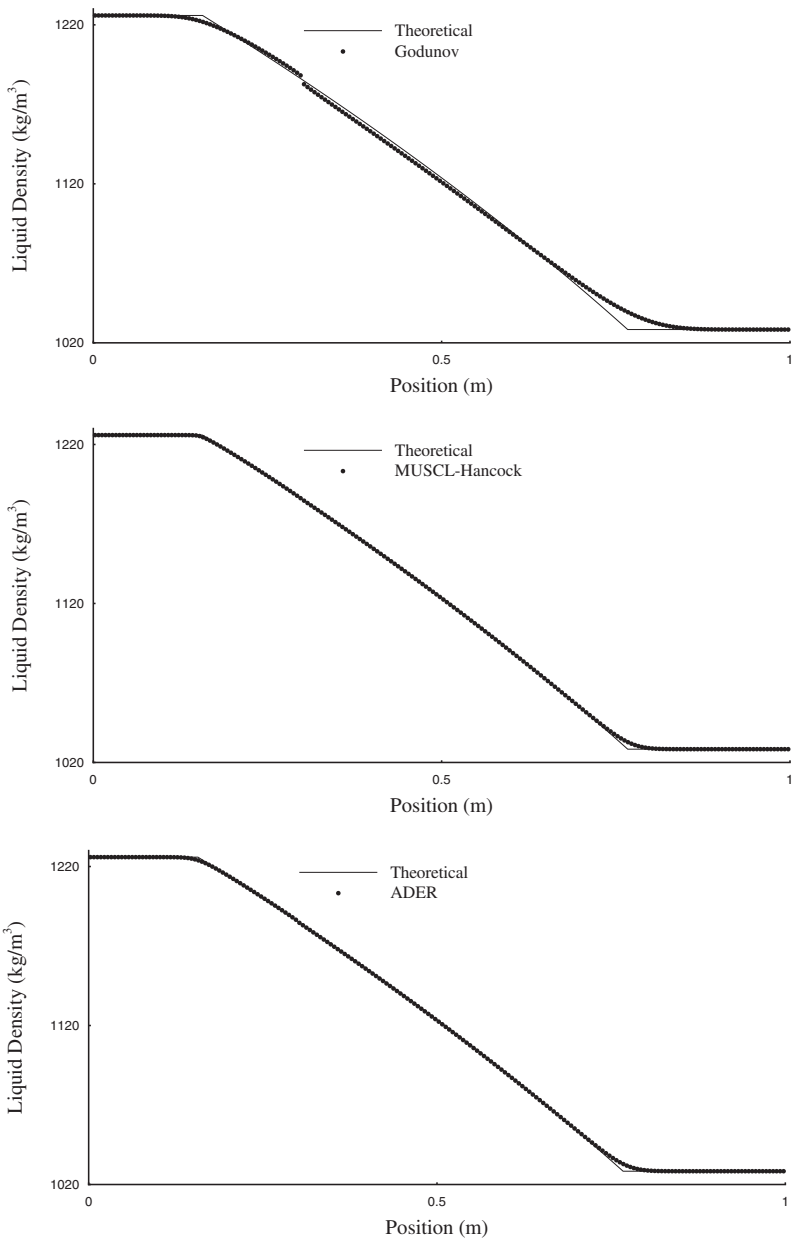


Figure 15. TEST 4: Numerical results for liquid density (symbols) from three numerical methods (Godunov, MUSCL_Hancock and ADER) are compared with the theoretical solution (line). CFL coefficient used is $C_{\text{cfl}} = 0.9$ and mesh used is $M = 200$ cells.

 

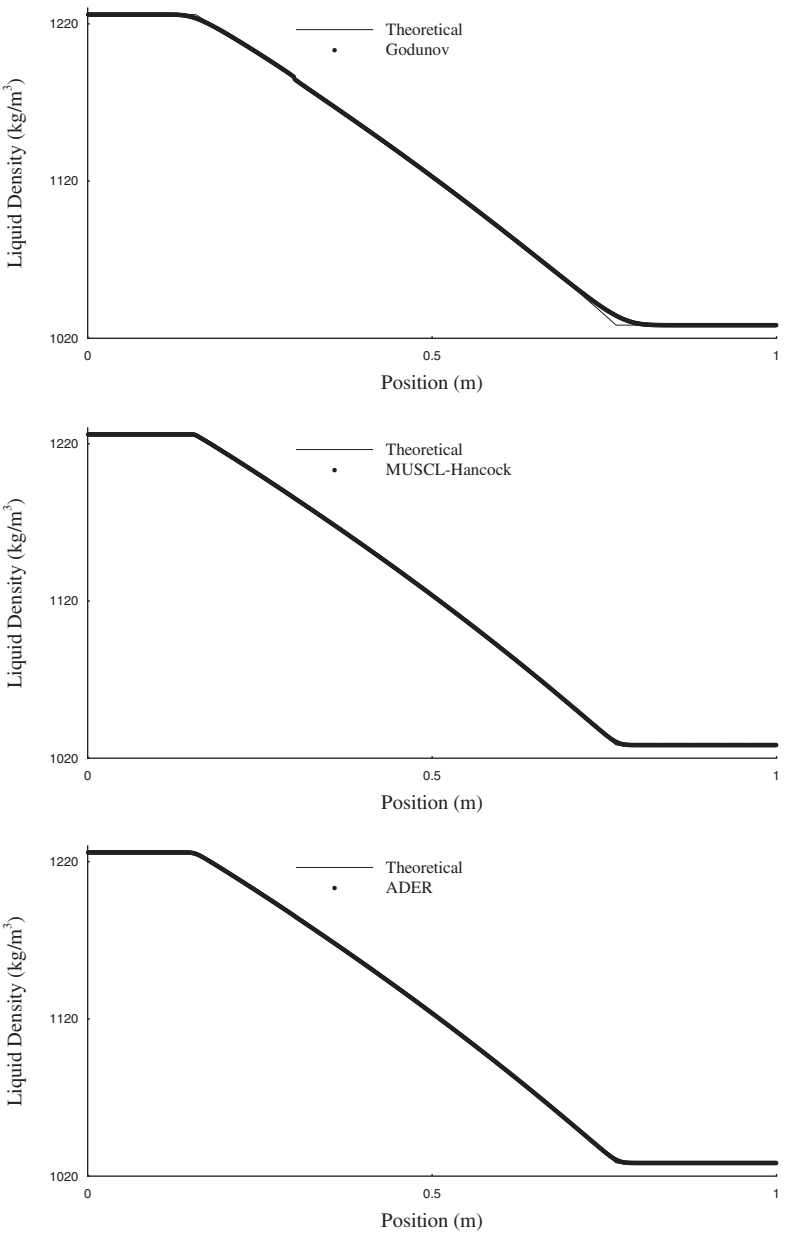


Figure 16. TEST 4: Numerical results for liquid density (symbols) from three numerical methods (Godunov, MUSCL_Hancock and ADER) are compared with the theoretical solution (line). CFL coefficient used is $C_{\text{cfl}} = 0.9$ and mesh used is $M = 800$ cells.

 

Results for Test 1 for liquid density are shown in Figures 4–6 for three different methods, namely the non-conservative Godunov first-order upwind, the non-conservative MUSCL_Hancock and the non-conservative ADER. As the mesh is refined we observe that the numerical results appear to converge to the theoretical solution. As expected, the first-order method converges more slowly. For this test problem there are no discontinuities in the solution and the agreement between the numerical and theoretical solutions is overall very satisfactory.

Results for Test 2 for liquid density are shown in Figures 7–10. For this test problem there is one discontinuity, namely a contact discontinuity. We observe that this is a more demanding test for all methods considered. The second-order non-linear methods still show some degree of spurious oscillations and even on the final mesh it is clear that the converged solution has not yet been reached. The reconstruction and limiting is performed component wise using physical variables. Characteristic limiting should improve the second-order results. Figure 10 shows separate results for the volume fraction, which changes only (discontinuously) across the contact discontinuity. For this quantity the performance of the numerical method is very satisfactory, the discontinuity is sharp and there are no spurious oscillations. The volume fraction positivity is always an important issue when it comes to numerical computations. At the first-order level, our first-order scheme preserves positivity. At the higher order level we utilize non-linear schemes, such as TVD schemes (or ENO or WENO schemes). Our experience is that positivity is preserved in all cases considered. See, for example Figure 10.

Results for Test 3 for liquid density are shown in Figures 11–13. This test problem consist of four shock waves (weak) and a trivial contact discontinuity. The theoretical solution is not strictly valid. However, it is remarkable to see the good agreement between the numerical and theoretical solutions. The second-order non-linear methods are free from spurious oscillation and the discontinuities are well resolved.

Results for Test 4 for liquid density are shown in Figures 14–16. This test problem has been constructed so that the solution consists of a single, isolated, rarefaction wave with a sonic point, for which the theoretical solution is exact. The point of this test is that sonic flows create difficulties to numerical methods, requiring special entropy fixes for some well known numerical schemes, particularly those based on linearized Riemann solvers. It is seen that the analogue of the Godunov first-order upwind method shows the typical *entropy glitch*. This is more evident in the coarse mesh, see Figure 14. As expected, the *entropy glitch* tends to disappear as the mesh is refined, see Figure 16. The second-order results do not seem to be affected by the presence of the sonic point.

## 7. SUMMARY AND CONCLUSIONS

We have presented a direct theoretical solution to the Riemann problem for the five-equation two-phase non-conservative model of Saurel and Abgrall and have then utilized this solution in the construction of upwind non-conservative methods to solve the general initial-boundary value problem for the two-phase flow model in non-conservative form. The basic upwind scheme constructed is the non-conservative analogue of the Godunov first-order upwind method. Second-order methods in space and time have then been constructed via the MUSCL and ADER approaches. The methods have been systematically assessed via a series of test problems with theoretical solutions. The theoretical solution given is thus used in

 

two ways (i) as a reference solution to assess the accuracy of numerical methods for some special test problems, and (ii) to construct upwind numerical methods to solve more general problems.

ACKNOWLEDGEMENTS

The first author acknowledges the financial support of the Department of Civil and Environmental Engineering of the University of Trento, Italy. The second author acknowledges the support provided by the Isaac Newton Institute for Mathematical Sciences, University of Cambridge, UK, as coorganizer of the six-month program on Non-Linear Hyperbolic Waves in Phase Dynamics and Astrophysics, January–July 2003, and the associated EPSRC senior visiting fellowship, Grant GRN09276.

REFERENCES

1. Stewart BH, Wendroff B. Two-phase flow: models and methods. *Journal of Computational Physics* 1984; **56**:363–409.
2. Drew D, Passman S. *Theory of Multicomponent Fluids*. Springer: New York, 1999.
3. Drew D. Mathematical modeling of two-phase flow. *Annual Review of Fluid Mechanics* 1983; **15**:261–291.
4. Ishii M. *Thermo-fluid Dynamic Theory of Two-phase Flow*. Eyrolles: Paris, 1975.
5. Saurel R, Abgrall R. A multiphase Godunov method for compressible multifluid and multiphase flows. *Journal of Computational Physics* 1999; **150**:425–467.
6. Baer M, Nunziato J. A two-phase mixture theory for the deflagration to detonation transition (DDT) in reactive granular materials. *International Journal of Multiphase Flow* 1986; **12**:861–889.
7. Romenski E, Toro EF. Compressible two-phase flows: two-pressure models and numerical methods. *Technical Report*, Isaac Newton Institute for Mathematical Sciences, 2004.
8. Toro EF. *Riemann Solvers and Numerical Methods for Fluid Dynamics* (2nd edn). Springer: Berlin, Heidelberg, 1999.
9. Andrianov N, Warnecke G. The Riemann problem for the Baer–Nunziato two-phase flow model. *Journal of Computational Physics* 2004; **195**:434–464.
10. Saurel R, Gavrilyuk S, Renaud F. A multiphase model with internal degree of freedom: application to shock-bubble interaction. *Journal of Fluid Mechanics* 2003; **495**:283–321.
11. Chinnayya A, Daniel E, Saurel R. Computation of detonation waves in heterogeneous energetic materials. *Journal of Computational Physics* 2004; **196**:490–538.
12. Thompson PA. *Compressible Fluid Dynamics*. McGraw-Hill: New York, 1972.
13. Jeffrey A. *Quasilinear Hyperbolic Systems and Waves*. Pitman: London, 1976.
14. Toro EF. Primitive, conservative and adaptive schemes for hyperbolic conservation laws. In *Numerical Methods for Wave Propagation*, Toro EF, Clarke JF (eds). Kluwer Academic Publishers: Dordrecht, 1998.
15. Toro EF, Siviglia A. PRICE: primitive centred schemes for hyperbolics systems. *International Journal for Numerical Methods in Fluids* 2003; **42**:1263–1291.
16. Toro EF, Millington RC, Nejad LAM. Towards very high order Godunov schemes. In *Godunov Methods*: *Theory and Applications*, Toro EF (ed.). Kluwer Academic Publishers: Dordrecht, 2001.
17. van Leer B. On the relation between the upwind-differencing schemes of Godunov, Enguist–Osher and Roe. *SIAM Journal on Scientific and Statistical Computing* 1985; **5**(1):1–20.

 